Impact of Rotor Segmentation on Electromagnetic Performance of PM Machine

Bhuvan Khoshoo
Department of Electrical &
Computer Engineering
Michigan State University East
Lansing, MI USA
khoshoob@msu.edu

Orwell Madovi

Department of Electrical &

Computer Engineering

Michigan State University East

Lansing, MI USA

madovior@msu.edu

Anmol Aggarwal
Department of Electrical &
Computer Engineering
Michigan State University East
Lansing, MI USA
aggarw43@msu.edu

Shanelle N. Foster
Department of Electrical &
Computer Engineering
Michigan State University East
Lansing, MI USA
hogansha@egr.msu.edu

Abstract—Rotor segmentation in a permanent magnet (PM) machine can present opportunities for cost reduction. However, the presence of flux gaps between the segments may seriously impact the machine's performance. This work proposes a general theory to assess the impact of rotor segmentation on the machine performance. The proposed theory states that for a given design constraint, the reluctance torque of the PM machine with rotor segmentation increases compared to the conventional machine. The proposed theory is validated using finite element simulations using two different machine designs, both at no-load and on-load operating conditions.

Index Terms—Electric Machines, Rotor Segmentation, PMSM, Reluctance Path, Flux Gap.

I. INTRODUCTION

The continuously growing interest in electrification of automotive systems to reduce carbon footprint and tailpipe emissions has resulted in the development of various machine topologies for hybrid and electric vehicles over the last two decades. Permanent magnet synchronous machines (PMSMs) are favorable over other machine types due to their high torque density and efficiency over wide speed range applications. However, PMSMs are typically more expensive than other electrical machine types due to costly rare earth permanent magnet (PM) material. Continuous efforts have also been made to reduce the dependency of PMSMs on rare earth PM material. While reducing rare earth material reduces cost, it also results in lower torque and power density of the machine. Therefore, other pathways must be explored to reduce the machine cost with minimal impact on machine performance.

In conventional manufacturing, a single sheet is punched to obtain both stator and rotor lamination and the remaining material is considered waste. Segmentation of electrical steel laminations can help reduce production cost by improving the sheet utilization factor [1], [2]. Segmentation also allows the use of oriented steel to improve the permeability in high saturation regions to reduce losses. Segmentation of the stator

This material is based upon work supported by the National Science Foundation under Grant No. 2045776.

is an efficient technique to improve the slot fill factor and ease the assembly process in the case of concentrated windings. Stator segmentation also offers isolation of phase windings, which is helpful during repair in case of faults that can cause serious damage to both machine and humans [3]–[5].

Use of segmented rotor laminations can further reduce manufacturing cost reduction. However, it also poses some crucial challenges. Rotor segmentation can introduce flux gaps which affect the magnetic circuit and ultimately the machine's performance. The influence of flux gaps in segmented stators have been evaluated in literature [6]. However, such an analysis of rotor segmentation in PMSMs is missing in literature. This paper fills this research gap by proposing and validating a general theory to predict the influence of flux gaps on the electromagnetic performance of segmented rotor interior permanent magnet (IPM) machines.

The paper is organized as follows: Section II discusses related work. Section III proposes a general theory to assess the impact of rotor segmentation on the machine's performance. Section IV describes the finite element analysis (FEA) setup used in this study. Section V provides FEA results for noload and on-load operation. Finally, section VI summarizes the conclusions of this work.

II. RELATED WORK

In the late 1990s, segmented rotors in PMSMs were explored to improve the flux-weakening performance of the machine. A novel segmented rotor PMSM was presented in [7] and [8] where the authors studied the effect of placing flux barriers in order to obstruct q-axis flux. The flux barriers reduced the saturation of the machine by obstructing armature (q-axis) flux, which provided higher overload performance. However, to maintain rated performance the current density in the stator had to be increased. Additionally, this novel configuration reduced the reluctance torque of the machine. Moreover, the authors only considered three values of the flux barrier thickness hb: (1) hb = 0, (2) hb = hPM, and (3) hb = 2*hPM, where hPM is the thickness of the magnets. A better

understanding of the impact of changes in the flux barrier thickness in the case of a segmented rotor PM machine is required.

A similar idea was explored in [9], [10]. Flux barriers were used to obstruct q-axis flux and achieve a higher d-axis inductance (L_d) than q-axis inductance (L_q) . This specific machine type, called normal saliency permanent magnet (NSPM) machine, can offer better overload performance. Additionally, it can also provide better field-weakening (FW) performance, since the machine is mostly operated with positive or slightly negative d-axis current (I_d) , allowing the current vector to be sustained till higher speeds. These NSPM machines, further explored in [11], are a specific design and the analysis is not transferable to other machine topologies. Furthermore, the design does not employ actual segmentation as the flux barriers do not extend from the rotor inner diameter (ID) to the rotor outer diameter (OD).

Other studies involving segmented rotor PM machines include an investigation of the structural performance [12] and the use of oriented steel to improve the performance by reducing torque ripple of PMSMs [13]. In general, analysis of segmented rotor in a PM machine is predominantly neglected. A primary reason for this lack of attention can be attributed to the question of its practicality. Assembling a segmented rotor can present a challenge and the operation at high speed raises further structural integrity concerns. Despite these concerns, segmented rotor designs have been explored in safety-critical applications, such as aircraft [14]–[16]. However, none of the studies comprehensively analyze the influence of rotor segmentation on the electromagnetic performance of a PMSM.

III. PROPOSED GENERAL THEORY

The reluctance path theory [17] shows that the d-axis flux has a single path through the magnet, while the q-axis flux linkage has two separate paths, as shown in Fig. 1. The theory was used to explain the variation of flux linkages in case of a segmented stator IPM machine [18]. This paper expands the reluctance theory to explain the variation of flux linkages in a segmented rotor PMSM.

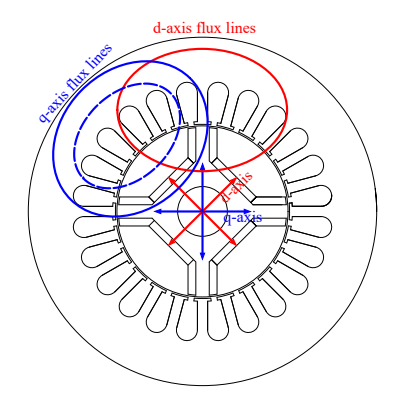


Fig. 1. IPMSM flux paths: primary reluctance path (solid blue), secondary reluctance path (dashed blue), and magnet flux path (solid red) [17].

In this work, two types of rotor segmentation are studied: (1) along d-axis, and (2) along q-axis, as shown in Fig. 2(a)

and Fig. 2(b), respectively. For each type of segmentation, the impact of different number of segments (N_s) and flux gap width (fg) are analyzed on no-load flux linkage (λ_{pm}) , d-axis flux linkage (λ_d) , q-axis flux linkage (λ_q) , average torque, and reluctance torque. The impact of rotor segmentation on machine flux linkages for no-load and on-load operation is explained below.

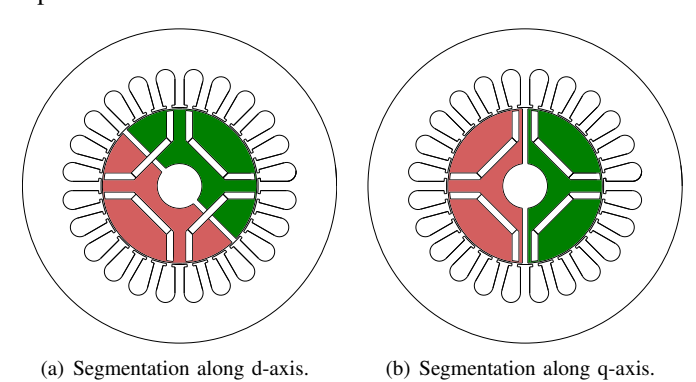


Fig. 2. Two types of rotor segmentation, along d-axis and along q-axis shown in (a) and (b) respectively for a 24-slot/4-pole IPM machine. Both machines have two N_s for each segmentation type as highlighted by different colours.

A. No-Load Operation

Permanent magnets are the only available source of magneto motive force (MMF) under no-load. Hence, no-load flux linkage is also called magnet-flux linkage (λ_{pm}), which flows through the d-axis flux path as shown in Fig. 3(a). The area of the d-axis flux path is directly proportional to the magnet pole arc, which is constant for a given machine design. Hence, the presence of flux gaps due to rotor segmentation along d-axis decreases the d-axis flux path area. Consequently, this leads to saturation of material close to flux gaps, as highlighted in Fig. 3(b). Therefore, λ_{pm} would decrease due to the presence of flux gaps when the rotor segmentation is performed in the d-axis direction. Moreover, the decrease becomes dominant with increased fg and N_s .

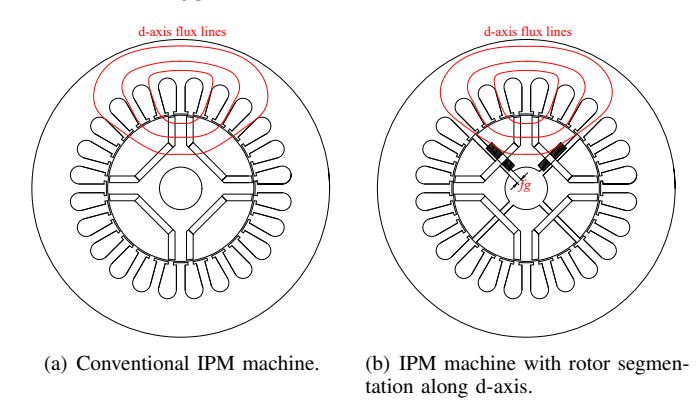


Fig. 3. Saturation on d-axis flux path due to rotor segmentation along d-axis.

Segmentation along the q-axis directly increases the reluctance of the d-axis flux path. The increased reluctance decreases λ_{pm} . Increasing N_s and fg further reduces λ_{pm} .

B. On-Load Operation

Segmentation along the d-axis increases the reluctance of the q-axis path, thereby decreasing λ_q . However, changes in λ_d , due to d-axis segmentation, depend on the change in the saturation level of the d-axis flux path, which depends on machine geometry. If the machine is less saturated along the d-axis path, as shown in Fig. 4(a), segmentation along d-axis would result in slightly increased λ_d . This results from the increased reluctance of the q-axis path leading to more flux to align along the d-axis path. However, as fg further increases, λ_d would decrease due to saturation on d-axis path close to flux gaps. Conversely, a heavily saturated d-axis flux path, as shown in Fig. 4(b), acts like a flux gap itself and prohibits an increase in λ_d . In fact, λ_d decreases due to saturation on the d-axis path due to non-zero flux gaps.

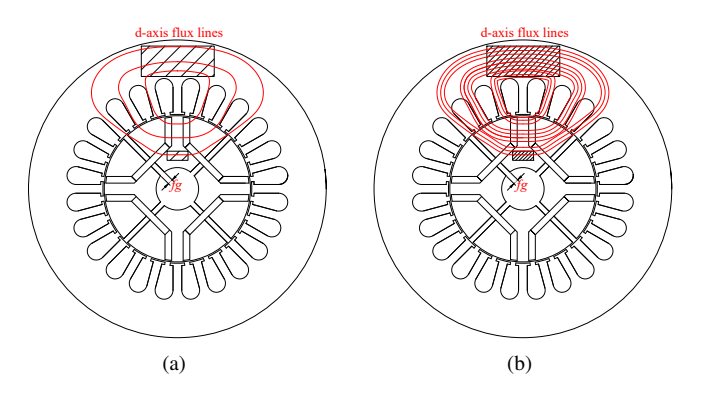


Fig. 4. Rotor segmentation along d-axis in IPM machine with less saturated d-axis flux path in (a) and highly saturated d-axis flux path in (b), respectively.

Rotor segmentation along q-axis increases the reluctance of the d-axis flux path. At low load, the q-axis flux linkage is low, and flux primarily flows through the d-axis flux path. Despite this, the introduction of flux gaps results in saturation of the q-axis width, which decreases λ_q , as highlighted in Fig. 5(b). Additionally, segmentation along the q-axis decreases λ_d due to increased reluctance of the d-axis path.

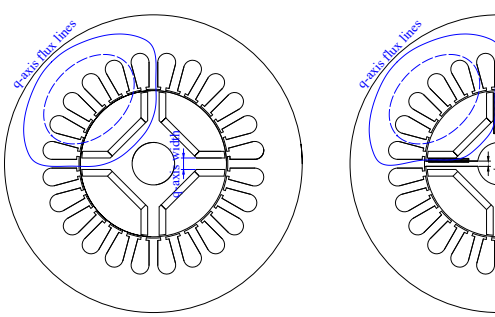


Fig. 5. Saturation on q-axis width due to rotor segmentation along q-axis.
Segmentation along q-axis in an IPM machine with small

q-axis width, when the machine is highly loaded, will saturate

(a) Conventional IPM machine. (b) IPM machine with rotor segmentation along q-axis.

the q-axis width quickly, increasing the reluctance of the q-axis path. For smaller values of fg, the reluctance increase of the q-axis path due to material saturation dominates the reluctance increase of the d-axis path consisting of magnets. This configuration will decrease λ_q but increase λ_d as more flux will concentrate along the d-axis. However, with a further increase in fg, λ_d would decrease due to a significant increase in the reluctance of the d-axis path.

On the other hand, if the machine has a large q-axis width, segmentation along q-axis has no significant change in the saturation level of the q-axis path compared to the reluctance increase of the d-axis path when the machine is highly loaded. Therefore, while λ_d will decrease, λ_q will increase as flux links with the q-axis path of less reluctance. This same effect is observed under demagnetization fault [19]. Furthermore, λ_q will continue increasing until the q-axis width is entirely saturated, leading to a significant increase in the reluctance of the q-axis path.

C. Impact of Segmentation on Synchronous Torque, Reluctance Torque, and Net Torque

Electromagnetic torque of an IPM machine comprises two components: synchronous torque and reluctance torque. The torque is given by (1), where the terms $\lambda_{pm}I_q$ and $(L_d-L_q)I_dI_q$ correspond to synchronous torque and reluctance torque, respectively. Also, p, I_d , and I_q represent the pole pairs of the machine, d-axis current, and q-axis current, respectively.

$$T = \frac{3}{2}p\left(\lambda_{pm}I_q + (L_d - L_q)I_dI_q\right) = \frac{3}{2}p\left(\lambda_dI_d - \lambda_qI_d\right)$$
(1)

Both types of segmentation, along the d- and q-axes, decrease synchronous torque due to a decrease in λ_{pm} . The reluctance torque of an IPM machine is directly proportional to the difference between L_q and L_d . Under certain design constraints, rotor segmentation along q-axis will increase the reluctance torque of the machine due to increased λ_q and decreased λ_d . Rotor segmentation will decrease net torque when both λ_d and λ_q decrease. Variation in the net torque is expected to be machine-specific.

IV. FINITE ELEMENT SETUP

Two IPM machines, IPM-A and IPM-B, are selected to analyze the influence of rotor segmentation. Some important parameters of the two machines are given in Table I. It is worth mentioning that the two selected IPM machines have different slot/pole combinations, magnet shape, magnet placement and q-axis width.

2-D models of the two conventional machines used for FEA are shown in Fig. 6(a) and Fig. 6(b), respectively. Since this study only analyzes effects due to rotor segmentation, the stator geometry for both machines remains unchanged. Details of the FEA setup are provided in Table II.

For each IPM machine used in this work, N_s is chosen such that the segmentation is symmetric, and each segment consists of at least one pole. This means that the value of N_s can vary from $N_s = 2$ to $N_s = N_p$, where N_p

TABLE I: PARAMETERS OF CONVENTIONAL MACHINES USED FOR ANALYSIS.

D4	Values		
Parameters	IPM-A	IPM-B	
Mechanical power (kW)	69	125	
Rated speed (RPM)	3000	4500	
Rated current (peak) (A)	177	565.7	
Magnet material	NdFeB	NdFeB	
Magnet layer	Single layer	Double layer	
Slot/pole	48/8	72/12	
Stack length (mm)	50.8	130	
Air-gap length (mm)	0.75	0.7	

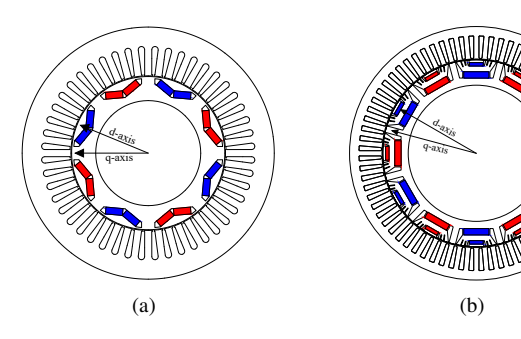


Fig. 6. Conventional IPM-A and IPM-B used in analysis in (a) and (b), respectively.

denotes the number of poles of machine. Furthermore, for both machines, the value of fg is varied from 0.1mm to 1mm. For all possible combinations of segmented rotor machines, their noload and on-load performance is compared to the conventional machines based on results obtained from transient magnetic FEA. All no-load analyses are carried out at the rated speed of the two conventional machines. Two cases are defined for on-load analysis: (1) 10% of the rated load and (2) 100% of the rated load. In both cases, machine performance is computed at the maximum torque per ampere (MTPA) angle. The excitation angle is varied from 90° to 180° in steps of 10° to estimate the MTPA angle. The complete setup for on-load analysis is summarized in Table III.

TABLE II: FINITE ELEMENT SETUP FOR ANALYSIS.

Variables	V	Values		
	IPM-A	IPM-B		
N_s	2,4,8	2,3,4,6,12		
<i>fg</i> (mm)	0.1, 0.25,	0.5, 0.75, 1		

TABLE III:
OPERATING CONDITIONS FOR ON-LOAD ANALYSIS.

Cases	Operating conditions		
Cases	Load (A)	Speed (RPM)	Mode
Case 1 Case 2	10% of rated 100% of rated	Rated Rated	MTPA MTPA
Case 2	100% of rated	Rated	MTI

V. FINITE ELEMENT RESULTS

The performance of each segmented rotor case is compared to the respective conventional IPM machine, without rotor segmentation. Here, the conventional machines, IPM-A and IPM-B are called A-Conven and B-Conven, respectively. A-Segd and A-Segq refer to IPM-A with segmentation along the d- and q-axis, respectively. Similarly, B-Segd and B-Segq refer to IPM-B with segmentation along the d- and q-axis, respectively.

A. No-Load Flux Linkages (λ_{pm})

The no-load flux density distributions of the two conventional machines are shown in Fig. 7(a) and Fig. 7(c), respectively. As explained previously, segmentation along daxis leads to material saturation close to flux gaps for both machines, as shown in Fig 7(b) and Fig. 7(d), respectively. Moreover, both types of segmentation lead to a decrease in λ_{pm} . As shown in Fig. 8, λ_{pm} decreases significantly after fg exceeds the machine's air gap length. It is worth mentioning that segmentation along q-axis impacts λ_{pm} more negatively due to a direct increase in the reluctance of the d-axis flux path, as shown in Fig. 9.

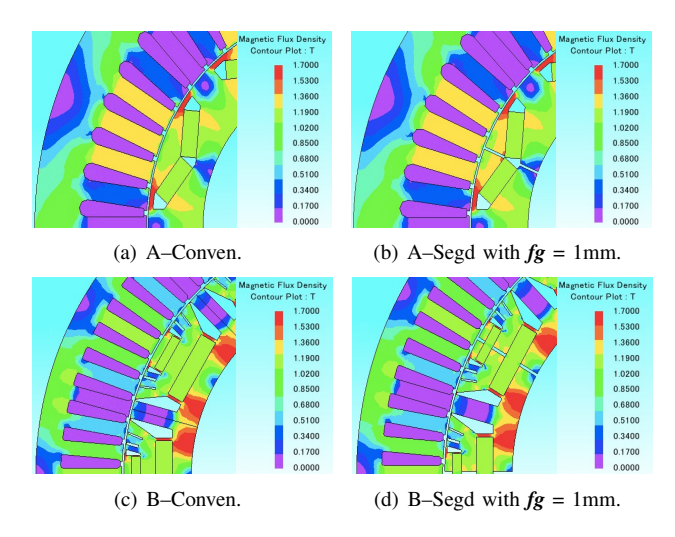


Fig. 7. No-load magnetic flux density plots highlighting material saturation close to flux gaps due to rotor segmentation along d-axis.

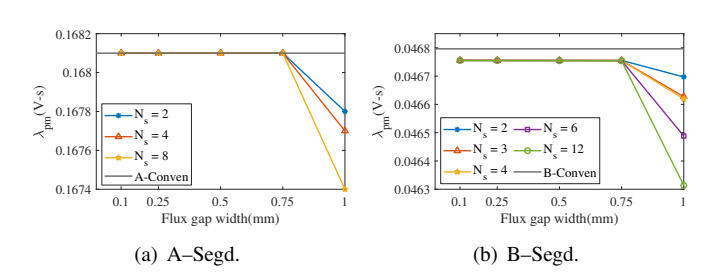


Fig. 8. Variation in λ_{pm} for segmentation along d-axis.

B. On-Load Flux Linkages (λ_d and λ_q)

Before analyzing the variation of flux linkages, it is helpful to examine the magnetic flux density plots and saturation

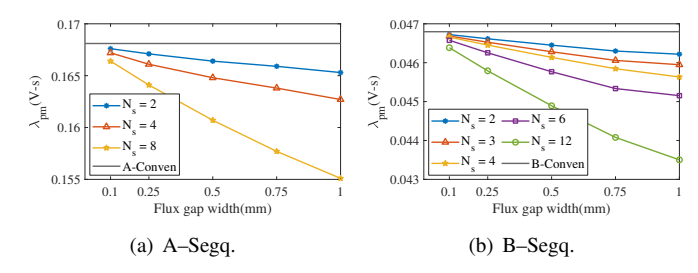


Fig. 9. Variation in λ_{pm} for segmentation along q-axis.

level of the two IPM machines at different loads. Clearly, the saturation level of the d-axis flux path of B-Conven is higher than that of A-Conven in both cases, as shown in Fig. 10. It is worth noting, A-Conven has larger q-axis width compared to B-Conven.

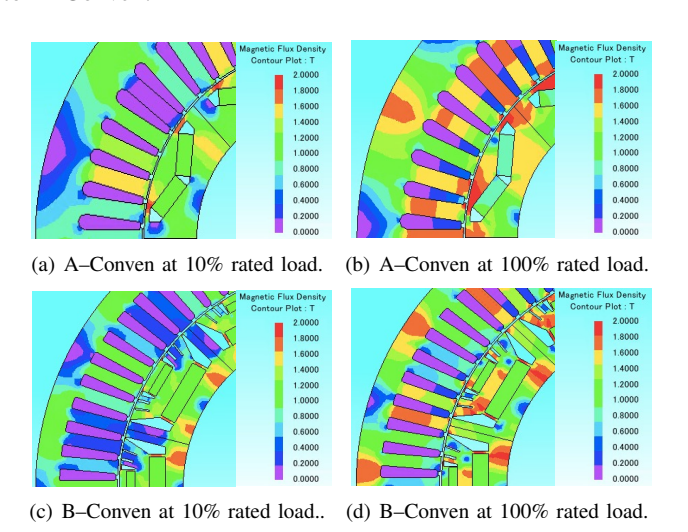
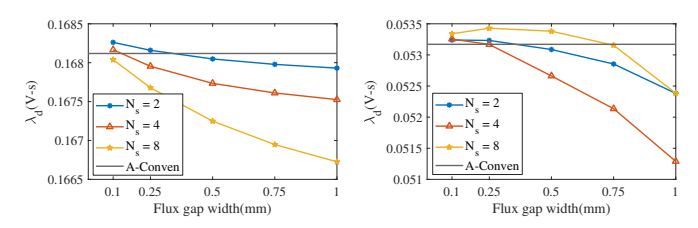


Fig. 10. Magnetic flux density plots at different load levels.

1) Segmentation along d-axis: Segmentation along d-axis for both machines due to the increased reluctance of the q-axis path leads to a decrease in the q-axis flux linkages. The reluctance of q-axis path increases with N_s and fg. On the other hand, variation in λ_d is dependent on the saturation level of the d-axis flux path, as explained in the previous section.

For both load levels, A–Segd results in a slightly increased λ_d compared to A–Conven with introduction of a small flux gap. This is due to lower saturation on the d-axis flux path, as shown in Fig. 11(a) and Fig. 11(b), respectively. This increase is more prominent when a significant flux is linked through the q-axis at rated load operation. Moreover, λ_d decreases with further increase in fg due to material saturation close to flux gaps.

At 10% rated load, B-Segd leads to decreased λ_d compared to B-Conven, due to a heavily saturated d-axis flux path, as shown in Fig. 12(a). However, at rated load operation, λ_d initially decreases due to heavy saturation on the d-axis path but then increases for $N_s \geq 4$, as shown in Fig. 12(b). This increase results from significantly decreased L_q due to increased reluctance of the q-axis path. This change in

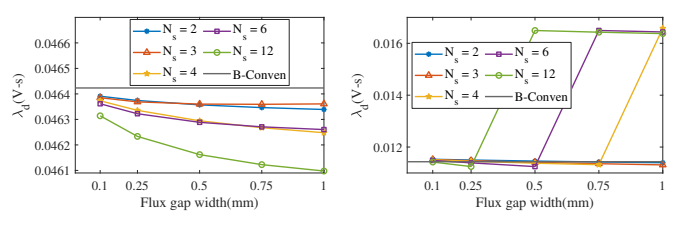


(a) Operation at 10% of rated load. (b) Operation at 100% of rated load.

Fig. 11. Variation in λ_d for A–Segd.

reluctance forces the MTPA angle, given by (2), to decrease. The decrease in the MTPA angle results in a sudden increase in λ_d .

$$\delta_{MTPA} = \cos^{-1}\left(\frac{-\lambda_{pm} + \sqrt{\lambda_{pm}^2 + 8I_s^2(L_d - L_q)^2}}{4(L_d - L_q)I_s}\right)$$
(2)



(a) Operation at 10% of rated load. (b) Operation at 100% of rated load.

Fig. 12. Variation in λ_d for B-Segd.

2) Segmentation along q-axis: At 10% of rated load, both machines A-Segq and B-Segq result in decreased λ_d and λ_q compared to A-Conven and B-Conven, as shown in Fig. 13 and Fig. 14, respectively.

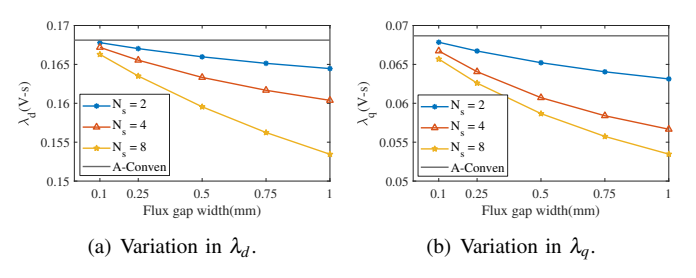


Fig. 13. Variation of flux linkage at 10% rated load for A-Segq.

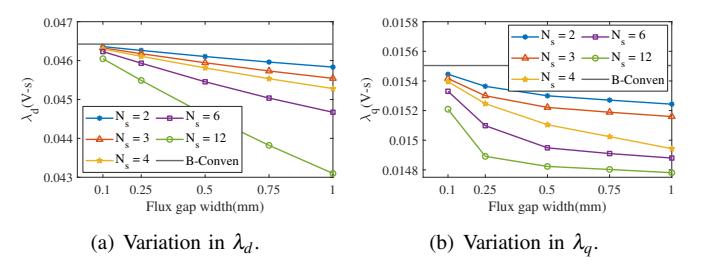


Fig. 14. Variation of flux linkage at 10% rated load for B-Segq.

Conversely, at 100% of the rated load, variations in λ_d and λ_q are impacted by the q-axis width of the machine.

Due to large q-axis width, A-Segq leads to a decrease in λ_d but an increase in λ_q at rated load operation as shown in Fig. 15. This is a result of more flux concentrating on the q-axis due to the increased reluctance of the d-axis path. It is worth mentioning that λ_q ceases to increase when the reluctance of the q-axis path, due to saturation of the q-axis width, begins to dominate.

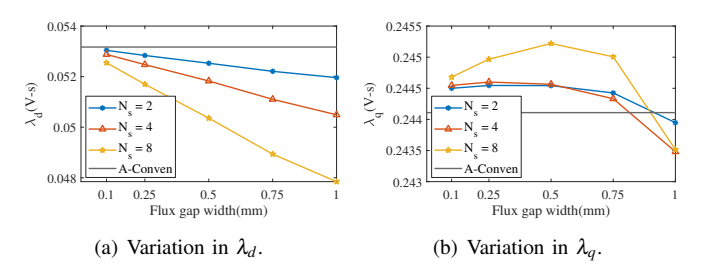


Fig. 15. Variation of flux linkage at 100% rated load for A-Segq.

On the other hand, B–Segq, with small q-axis width, results in an increased λ_d and decreased λ_q at rated load operation, as shown in Fig. 16. This results from more flux aligning with the d-axis as the q-axis width quickly saturates due to non-zero flux gaps.

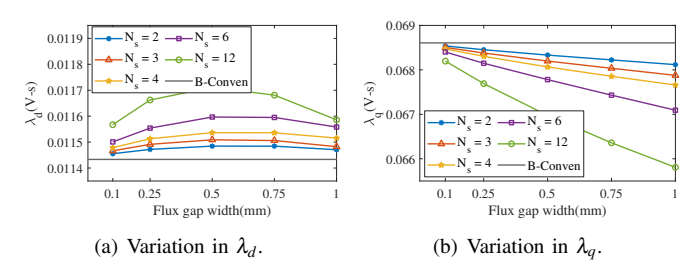


Fig. 16. Variation of flux linkage at 100% rated load for B-Segq.

C. Average Torque and Reluctance Torque

Compared to the conventional machines, both types of rotor segmentation decrease average torque which increases with N_s and fg, as shown in Fig. 17. However, it is worth mentioning that for any N_s at rated load, the change in average torque is less than 1% for A-Segq and B-Segq, and less than 3% for A-Segd and B-Segd, when fg is less than 40% of the air-gap length. Additionally, it is observed that there is a trade-off between the type of segmentation and the load level of the machine, as shown in Table IV. For lower load levels, segmentation along the d-axis is more advantageous, whereas, for higher load levels, segmentation along the qaxis gives better performance. At lower load levels, magnets are the primary source of MMF and average torque. Hence, segmentation along q-axis will lead to obstruction of d-axis flux, decreasing magnet torque. On the other hand, placing flux gaps along the d-axis leads to obstruction of q-axis flux at higher load levels, decreasing the reluctance torque of the machine.

Moreover, at rated load, A-Segq increases the reluctance torque compared to A-Conven, as shown in Fig. 18. This is

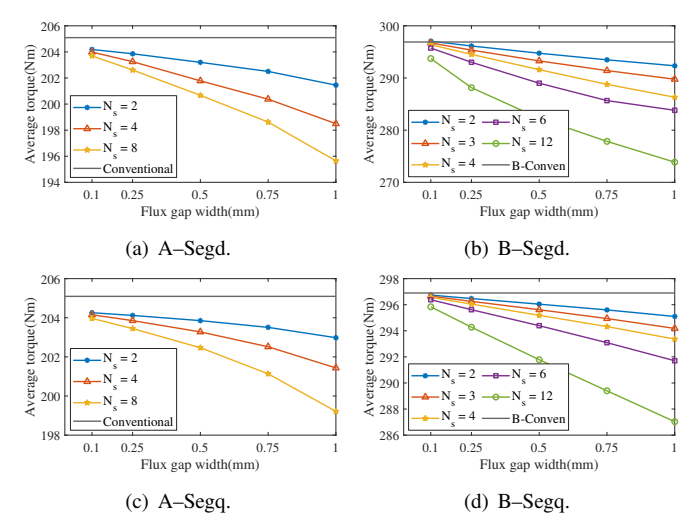


Fig. 17. Variation in average torque at 100% rated load.

TABLE IV: Average torque decrease for $m{N_s} = m{N_p}$ and $m{fg} = 0.5$ mm.

	10% rated load		100% rated load	
Machine	Segment.	Segment.	Segment.	Segment.
	along d-axis	along q-axis	along d-axis	along q-axis
IPM-A	2.62%	6.58%	2.15%	1.28%
IPM-B	1.82%	3.92%	4.92%	1.72%

due to improvement in the saliency of the machine owing to increased λ_q and decreased λ_d as shown in Fig. 15. To gain further insights into the impact of segmentation along q-axis, the performance of the following designs is compared in the complete torque-speed envelope:

- (i) A-Conven
- (ii) A-Segq, with $N_s = N_p$ and fg = 0.1mm
- (iii) A-Segq, with $N_s = N_p$ and fg = 0.5mm

All three cases have the same base speed, as shown in Fig. 19(a). Moreover, the segmented machines deliver similar performance to the conventional machine in the entire torque/speed region. In fact, A–Segq with fg=0.1mm produces slightly larger torque in flux weakening region than A–Conven. Additionally, while A–Segq with fg=0.5mm produces slightly less torque than A–Conven, it is able to reach slightly higher speed. This slight performance improvement is due to an

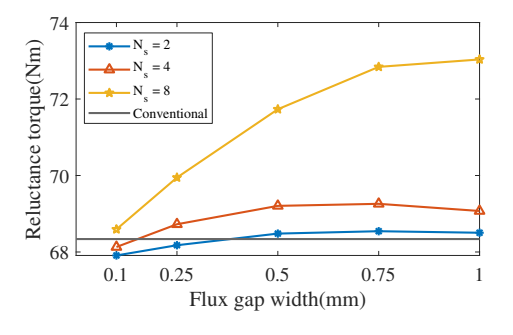


Fig. 18. Increased reluctance torque of A-Segq at 100% rated load.

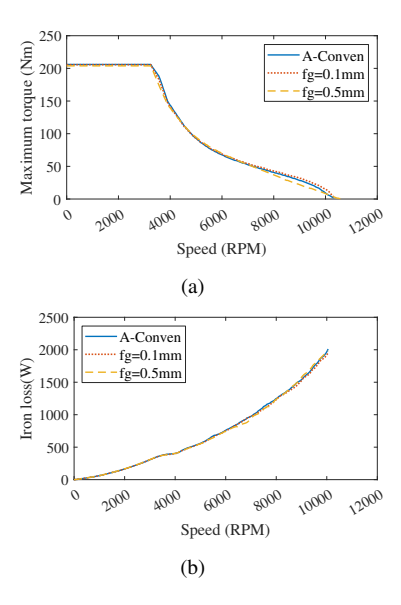


Fig. 19. Torque/speed profile of compared cases in (a) and Iron-loss profile at maximum achievable torque in (b).

improvement in the saliency of the segmented machine as flux gaps on the q-axis obstruct the d-axis flux. Additionally, all three cases also have similar iron loss profile at the maximum achievable torque in the speed range, as shown in Fig. 19(b).

VI. CONCLUSION

In this work, the impact of rotor segmentation on the electromagnetic performance of interior permanent magnet (IPM) machines has been analyzed. A general theory has been presented to investigate the impact of rotor segmentation on no-load flux linkages, d/q-axis flux linkages, average torque, and reluctance torque of IPM machines. The proposed theory has been successfully validated with finite element results at no-load and on-load operation obtained from two different IPM machines with different slot/pole combinations, magnet shapes, magnet placement, and material saturation level. It has been observed that rotor segmentation can be implemented in IPM machines without significant loss of average torque.

It has been shown that under certain conditions, segmentation along q-axis increases the reluctance torque of an IPM machine which is also reflected in slightly improved performance in the flux-weakening region. This phenomenon can be further explored to improve the design of IPM machines, to achieve higher torque during short circuit fault mitigation, which typically involves suppression of magnet flux.

The two types of segmentation on the d- and q-axes lead to a performance trade-off at different load levels. Further investigations are required to analyze the trade-off between machine performance and the extent of segmentation. Moreover, a thermal analysis should be included to examine the demagnetization of permanent magnets resulting from localized hot-spots due to increased material saturation.

REFERENCES

[1] A. Aggarwal, E. G. Strangas, and A. Karlis, "Review of segmented stator and rotor designs for ac electric machines," in 2020 International

- Conference on Electrical Machines (ICEM), vol. 1, 2020, pp. 2342–2348.
- [2] T. Albrecht, C. Gürsel, E. Lamprecht, and T. Klier, "Joining techniques of the rotor segmentation of pm-synchronous machines for hybrid drives," in 2012 2nd International Electric Drives Production Conference (EDPC), 2012, pp. 1–8.
- [3] S. Huang, A. Aggarwal, E. G. Strangas, K. Li, F. Niu, and X. Huang, "Robust stator winding fault detection in pmsms with respect to current controller bandwidth," *IEEE Transactions on Power Electronics*, vol. 36, no. 5, pp. 5032–5042, 2021.
- [4] S. Huang, E. G. Strangas, A. Aggarwal, K. Li, and F. Niu, "Robust interturn short-circuit detection in pmsms with respect to current controller bandwidth," in 2019 IEEE Energy Conversion Congress and Exposition (ECCE), 2019, pp. 3897–3904.
- [5] S. Huang, A. Aggarwal, E. G. Strangas, B. Khoshoo, K. Li, and F. Niu, "Mitigation of interturn short-circuits in ipmsm by using mtpcc control adaptive to fault severity," *IEEE Transactions on Power Electronics*, vol. 37, no. 4, pp. 4685–4696, 2022.
- [6] G. J. Li, Z. Q. Zhu, W. Q. Chu, M. P. Foster, and D. A. Stone, "Influence of flux gaps on electromagnetic performance of novel modular pm machines," *IEEE Transactions on Energy Conversion*, vol. 29, no. 3, pp. 716–726, 2014.
- [7] D. Ionel, J. Eastham, and T. Betzer, "Finite element analysis of a novel brushless dc motor with flux barriers," *IEEE Transactions on Magnetics*, vol. 31, no. 6, pp. 3749–3751, 1995.
- [8] D. Ionel, M. Balchin, J. Eastham, and E. Demeter, "Finite element analysis of brushless dc motors for flux weakening operation," *IEEE Transactions on Magnetics*, vol. 32, no. 5, pp. 5040–5042, 1996.
- [9] N. Bianchi and S. Bolognani, "Performance analysis of an ipm motor with segmented rotor for flux-weakening applications," in 1999. Ninth International Conference on Electrical Machines and Drives (Conf. Publ. No. 468), 1999, pp. 49–53.
- [10] N. Bianchi, S. Bolognani, and B. Chalmers, "Salient-rotor pm synchronous motors for an extended flux-weakening operation range," *IEEE Transactions on Industry Applications*, vol. 36, no. 4, pp. 1118–1125, 2000.
- [11] M. Fontana and N. Bianchi, "Design and analysis of normal saliency ipm spoke motor," *IEEE Transactions on Industry Applications*, vol. 56, no. 4, pp. 3625–3635, 2020.
- [12] F. Lorenz, R. Werner, D. Paul, and T. Stein, "Circumferentially segmented rotor architecture for pmsm traction machines," in 2020 International Conference on Electrical Machines (ICEM), vol. 1, 2020, pp. 2260–2265.
- [13] S. Taghavi and P. Pillay, "A novel grain-oriented lamination rotor core assembly for a synchronous reluctance traction motor with a reduced torque ripple algorithm," *IEEE Transactions on Industry Applications*, vol. 52, no. 5, pp. 3729–3738, 2016.
- Y. Loh, M. A. Prabhu, Wang, Viswanathan, and S. Ramakrishna, "Optimal segmented embedded electrical design for the machine electric aircraft," The Journal of Engineering, vol. more no. 17, pp. 4321–4324, 2019. [Online]. Available: https://ietresearch.onlinelibrary.wiley.com/doi/abs/10.1049/joe.2018.8192
- [15] S. Ullah, S. P. McDonald, R. Martin, M. Benarous, and G. J. Atkinson, "A permanent magnet assist, segmented rotor, switched reluctance drive for fault tolerant aerospace applications," *IEEE Transactions on Industry Applications*, vol. 55, no. 1, pp. 298–305, 2019.
- [16] A. Zulu, B. C. Mecrow, and M. Armstrong, "Permanent-magnet flux-switching synchronous motor employing a segmental rotor," *IEEE Transactions on Industry Applications*, vol. 48, no. 6, pp. 2259–2267, 2012.
- [17] S. Hayslett and E. Strangas, "Analytical Design of Sculpted Rotor Interior Permanent Magnet Machines," *Energies*, vol. 14, no. 16, 2021. [Online]. Available: https://www.mdpi.com/1996-1073/14/16/5109
- [18] A. Aggarwal, M. Meier, E. Strangas, and J. Agapiou, "Analysis of modular stator pmsm manufactured using oriented steel," *Energies*, vol. 14, no. 20, p. 6583, Oct 2021.
- [19] R. Z. Haddad, C. A. Lopez, S. N. Foster, and E. G. Strangas, "A voltage-based approach for fault detection and separation in permanent magnet synchronous machines," *IEEE Transactions on Industry Applications*, vol. 53, no. 6, pp. 5305–5314, 2017.